MedCrave
Step into the World of Research
Material Science & Engineering International Journal

Review Article

Open Access
CrossMark

Computation and field dynamic stress simulation of shovel crawler shoes

Abstract

Large capacity electric cable shovels are widely used in surface mining of Athabasca oil sands formation to meet economic production targets. The capital investments and operating costs of these shovels are high due to the abrasive nature of the oil sands formation. The interaction of the crawler tracks of the shovel with the abrasive oil sands formation during shovel propel and loading operation can cause large dynamic stresses in the crawler shoes of the shovel. The study of the dynamic stress distribution in the crawler shoes is important to understand crack initiation, propagation and premature fatigue failure of shoes. This paper develops a multi-body dynamic 3-D virtual prototype model of the rigid-flexible crawler track assembly interacting with oil sands formation to establish the dynamic stress distribution in the crawler shoes of the P&H 4100 BOSS shovel during its propel and loading duty cycles. The field data available for cyclic ground pressure under the shovel during the loading operation is then applied as an input into the 3-D virtual prototype model of the rigid-flexible crawler track assembly to capture the model dynamics and real-time stresses and deformation of flexible crawler shoes within MSC.ADAMS. The flexible crawler shoes are generated in the FEA program MSC.NASTRAN and imported into MSC ADAMS. The simulation results show large fluctuating contact forces developing at the interface between the crawler shoes and oil sands terrain causing large fluctuating stresses in the flexible crawler shoes with a maximum von Mises stress of 79MPa during both propel and loading cycles. A further study is required to simulate the operations with realistic assumptions to provide a basis for subsequent wear, crack and fatigue life prediction of crawler shoes for extending service life of the crawlers.

Keywords: surface mining, crawler-terrain interactions, rigid-flexible multi-bodydynamic theory, virtual prototype simulation, field data, modal analysis, modal stress recovery

Special Issue - 2018

Samuel Frimpong, Magesh Thiruvengadam, Eric Gbadam
Department of Mining and Nuclear Engineering, Missouri University of Science and Technology, USA

Correspondence: Samuel Frimpong, Department of Mining and Nuclear Engineering, Missouri University of Science and Technology, Rolla, MO 65401, USA, Tel 573 34 4753, Email frimpong@mst.edu

Received: August 01, 2017 | **Published:** December 31, 2018

Introduction

Electric cable shovel excavator is widely used in the surface mining operations of oil sand and other highly abrasive formations. The oil sands mines in Alberta use P&H 4100C Boss shovel.[1,2] for their loading operations. The lower works of this shovel consist of propel and crawler systems.[3–7] The crawler system consists of a crawler track assembly, front and rear idlers, lower rollers and guide rails.[3] The crawler track assembly is made up of shoes that are connected together by link pins to form a continuous chain. The efficiency and reliability of the shovel during the excavation of oil sands depends on the service life of the crawler track. The two crawler tracks interact with the abrasive terrain and distribute the machine and dipper loads to the ground during both propel and loading duty cycles. This interaction generates dynamic loads which can cause stress loading, wear, and crack and fatigue failure of the crawler shoes. The only published study on dynamic stress simulation of shovel crawler shoes was conducted by Frimpong et al.[4–7] They developed the 3-D virtual prototype model of the rigid-flexible open chain crawler track assembly interacting with oil sands to study stress distribution in the crawler shoes during shovel propel and loading operations.

The load due to machine weight and dipper pay load were distributed on each crawler shoe based on the assumptions obtained from on-field observation. The cyclic ground pressure acting under the P&H 4100C Boss shovel during the loading duty cycle is reported in the field study undertaken by Joseph,[8] Joseph et al.,[9] & Sharif Abadi et al.[10] They measured ground bearing pressure acting under shovel front and rear track for three idealized shovel-truck loading duty cycles using passive seismic instrumentation. The present study uses the field data[8–10] to distribute load on the crawler track to determine dynamic stress distribution in the crawler shoes during propel and loading within MSC.ADAMS VIEW/FLEX/ DURABILITY and MSC.NASTRAN.[11–15] This stress results can be used in the subsequent study of crawler shoes for investigating its crack and fatigue failure.

Geometry of the crawler track and load distribution

Frimpong et al.,[4–7] developed the open chain crawler track assembly made up of 13 crawler shoes in contact with the ground with track length of 8.37m. Sharif Abadi et al.,[10] used 9m as the length of the crawler track in contact with the ground for calculating the static ground pressure from a field study. The crawler track is also divided into front and rear components to represent cyclic ground bearing pressure acting under shovel during the loading duty cycle. This study uses the ground pressure measured under the shovel front and rear[8–10] as input load on each crawler shoe of the open crawler track chain to simulate stress distribution during propel and loading duty cycles. Another crawler shoe is added to the existing open chain from Frimpong et al.,[4–7] to

i. Increase the track length from 8.37m to 9.02m to match the track length in the field study.

ii. Divide track length equally into the front and rear parts each with 7 crawler shoes.

Figure 1 shows the modified crawler track assembly model divided into front and rear parts comprising 14shoes in contact with the oil sands terrain. The material properties of crawler shoes and oil sand units are illustrated in Table 1. The crawler shoes 1-14 (numbered in blue) and 247 oil sands units are identified using Part numbers 2-262 as shown in Figure 1. Part 1 is the default ground link in MSC.ADAMS. The global coordinate system is located at point O and is shown in Figure 2. The geometry of the modified crawler track assembly is imported into MSC.ADAMS to develop rigid-flexible virtual prototype model of crawler-terrain interaction. The joint constraint equations for crawler shoes and oil sand units, and motion constraint equations for driver crawler shoe 14 and each spring damper oil sand mass units can be found in Frimpong et al.[4–7] The stiffness (k) and damping (c) of the oil sands unit are listed in Table 1. The motion constraint on driver crawler shoe 14, which can cause the crawler track to accelerate, move at constant speed and decelerate, is deactivated when the loading cycle begins to allow six-DOF free crawler movement. The contact forces between crawler shoes and terrain is estimated using parameters in Table 2. The load distribution on crawler shoes on the front and rear parts estimated from the field study[8–10] is shown in Figure 1. More details on the external forces applied on the crawler shoes can be found in Frimpong et al.[4–7]

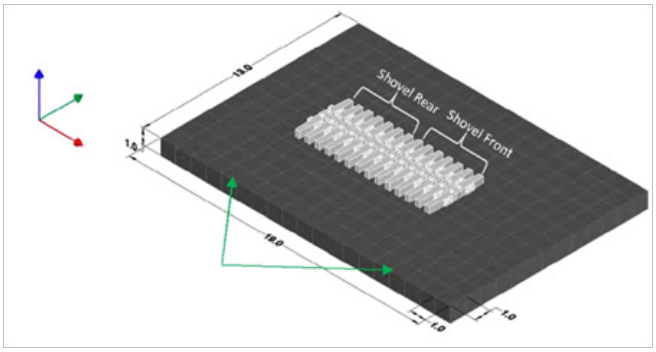

Figure 1 Modified crawler track- oil sand assembly.

Ground pressure under the shovel

The ground pressure acting under the shovel for three loading duty cycles for front and rear[8–10] is shown in Figure 2. It takes approximately 45 seconds to complete one duty cycle. Each duty cycle consists of digging, hoisting, swinging from the face and dumping into a spotted haul truck, and swinging back to the digging face to start the next duty cycle. During propel the pressure load on the front and rear crawler shoes are same and is due to empty shovel weight without dipper load. The total machine weight for the P&H 4100C BOSS is 1,410,184kg.[1] The total area of contact between shovel and ground is 2x9mx3.51m=63.18m^2. The static ground pressure due to machine weight is given in equation (1).

Table 1 Material Properties of System[16,17]

Body	Density (kg/m^3)	Mass (kg)	Elastic Modulus	Poisson's Ratio	Stiffness (k) MN/m	Damping (c) (kNs/m)
Crawler Shoe	7847.25	4489.63	200 GPa	0.3	-	-
Oil-sand	1600.0	1600	20 Mpa	0.3	20	120

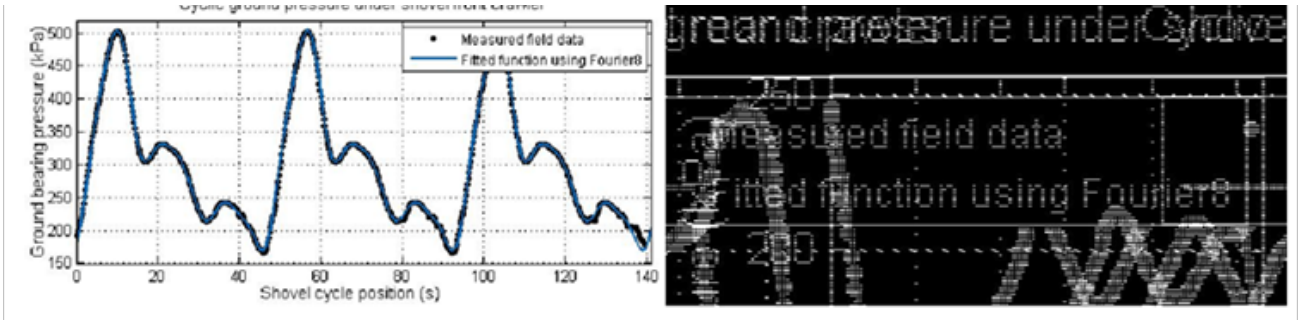

Figure 2 Cyclic ground pressure under shovel front and rear crawler track.8–10

Table 2 Contact parameters used in the study7

Normal force		Friction force	
Contact Stiffness (k, N/m)	1.00E+08	Static Coefficient (μ_s)	0.5
Max. Contact Damping (c_{max}, N-s/m)	1.00E+04	Dynamic Coefficient (μ_d)	0.3
Force Exponent (e)	1.5	Static transition velocity (V_{st}, m/s)	0.01
Max. Penetration Depth (d, m)	1.00E-04	Dynamic transition velocity (V_d, m/s)	0.1

Citation: Frimpong S, Thiruvengadam M, Gbadam E. Computation and field dynamic stress simulation of shovel crawler shoes. *Material Sci & Eng.* 2018;2(6):241–250. DOI: 10.15406/mseij.2018.02.00065

P_s =[(1410184kgx9.81m/s^2) 63.18m^2]=218.960kPa (1)

During loading the ground pressure acting under the front and rear crawler tracks (Figure 2) can be distributed uniformly as pressure loads on the respective seven front and rear crawler shoes (Figure 1).

This is achieved by fitting an appropriate curve to the measured ground pressure data using Fourier 8 function in Matlab. The fitted function for shovel front crawler is shown in equation (2).

$$P_F(t)=A_{0F}+A_{1F}+B_{1F}+A_{2F}+B_{2F}+A_{3F}+B_{3F}+A_{4F}+B_{4F}+A_{5F}+B_{5F}+A_{6F}+B_{6F}+A_{7F}+B_{7F}+A_{8F}+B_{8F} \quad (2)$$

Similarly the fitted function for shovel rear crawler is shown in equation (3).xin equations (4) and (5) is normalized using mean (μ) and standard deviation (σ) using equation (6).

$$P_R(t)=A_{0R}+A_{1R}+B_{1R}+A_{2R}+B_{2R}+A_{3R}+B_{3R}+A_{4R}+B_{4R}+A_{5R}+B_{5R}+A_{6R}+B_{6R}+A_{7R}+B_{7R}+A_{8R}+B_{8R} \quad (3)$$

$$A_{0F}=a_{0F};A_{1F}=a_{1F}\times\cos(x\times w_F);B_{1F}=b_{1F}\times\sin(x\times w_F);\quad A_{2F}=a_{2F}\times\cos\times(2\times x\times w_F);\quad B_{2F}=b_{2F}\times\sin(2\times x\times w_F)$$

$$A_{3F}=a_{3F}\times cos(3\times x\times w_F);\quad B_{3F}=b_{3F}\times sin(3\times x\times w_F);\quad A_{4F}=a_{4F}\times cos(4\times x\times w_F);\quad B_{4F}=b_{4F}\times sin(4\times x\times w_F) \quad (4)$$

$$A_{5F}=a_{5F}\times cos(5\times x\times w_F);\quad B_{5F}=b_{5F}\times sin(5\times x\times w_F);\quad A_{6F}=a_{6F}\times cos(6\times x\times w_F);\quad B_{6F}=b_{6F}\times sin(6\times x\times w_F)$$

$$A_{7F}=a_{7F}\times cos(7\times x\times w_F);\quad B_{7F}=b_{7F}\times sin(7\times x\times w_F);\quad A_{8F}=a_{8F}\times cos(8\times x\times w_F);\quad B_{8F}=b_{8F}\times sin(8\times x\times w_F)$$

$$A_{0R}=a_{0R};A_{1R}=a_{1R}\times cos(x\times w_R);B_{1R}=b_{1R}\times sin(x\times w_R);\quad A_{2R}=a_{2R}\times cos(2\times x\times w_R);\quad B_{2R}=b_{2R}\times sin(2\times x\times w_R)$$

$$A_{5R}=a_{5R}\times cos(5\times x\times w_R);\quad B_{5R}=b_{5R}\times sin(5\times x\times w_R);\quad A_{6R}=a_{6R}\times cos(6\times x\times w_R);\quad B_{6R}=b_{6R}\times sin(6\times x\times w_R) \quad (5)$$

$$A_{5R}=a_{5R}\times cos(5\times x\times w_R);\quad B_{5R}=b_{5R}\times sin(5\times x\times w_R);\quad A_{6R}=a_{6R}\times cos(6\times x\times w_R);\quad B_{6R}=b_{6R}\times sin(6\times x\times w_R)$$

$$A_{7R}=a_{7R}\times cos(7\times x\times w_R);\quad B_{7R}=b_{7R}\times sin(7\times x\times w_R);A_{8R}=a_{8R}\times cos(8\times x\times w_R);\quad B_{8R}=b_{8R}\times sin(8\times x\times w_R)$$

$$X=\frac{t-\mu}{\sigma} \quad (6)$$

t in equation (6) is the simulation time in seconds. The mean and standard deviation for shovel crawler front and rear track is shown in Table 3. The coefficients a_i, and b_i, (where i=1, 2 …8) and constants w_F, w_R in equations (4) and (5) are given in Table 4. The fitted curve from equations (2)-(6) is also plotted in Figure 3 and shows good comparison with measured field data.

Table 3 Mean and standard deviation

Quantity	Front crawler shoes	Rear Crawler Shoes
Mean (μ, s)	69.9	67.55
Standard Deviation (σ, s)	40.33	39.18

Load distribution on crawler shoes

The surface area of each crawler shoe A_s= 1.3331m^2. The pressure load/shoe in KN is calculated using

i. crawler shoe surface area;

ii. pressure values given in equations (1)-(3); and

iii. the ratio of the contact area between each track-terrain and total surface area of 14 crawler shoes.

The simulation time consists of

i. 15 seconds propel (0<t<15s); and

ii. 46.5 s loading duty cycle (18.5<t<65s) as in (Figure 3).

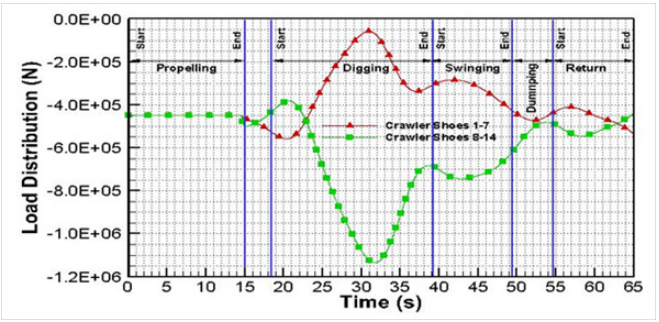

Figure 3 Load distributions on crawler shoes during shovel operation.

During propelling motion, the load distribution on the front and rear crawler shoes is calculated from static pressure load given in equation (1) minus crawler shoe weight in contact with the ground[5,7] which is Ps,mod ≈ 200kPa. This modified pressure load is distributed as uniform load in Newton on crawler shoes 1-14 as shown in Figure 3. Similarly, during loading (18.5 < t < 65 s), the pressure load acting on front crawler shoes (8-14) is calculated from equation (2) while for rear crawler shoes (1-7), the loads are obtained from equation (3). Only the part of the cycle ground curve between 40 and 90 seconds in

Figure 2 is used for simulation. This is because in the first 25 seconds, the shovel is brought to quasi-static equilibrium (time t=0, in Figure 3) and in the next 15 seconds, which is 0< t<15s in Figure 3, the shovel propel operation takes place under uniform pressure load. From Figure 3, the pressure loads at t=15 seconds for front track (P_F (t =15s)=223.55kPa) and for rear track (P_R (t=15s)=207.24kPa) are not equal to the uniform pressure load P_s,mod ≈ 200kPa acting on the crawler track during propel. To avoid discontinuity at t=15 seconds, the pressure load changes as a cubic function for a time period of 0.5 second (14.5 s to 15 s) from P_s,mod to the corresponding values for front and rear tracks as in (Figure 3). At t=15 seconds, the shovel completes the propel motion and from 15 to 18.5 seconds, it returns with empty dipper at corner position to empty dipper at the face as part of the first duty cycle in Figure 3. At t=18.5 seconds, the empty dipper engages the bank to begin the second digging operation. The duration for the second loading cycle from (Figure 3) is 46.5 seconds with return at t=65 s as in Figure 3. These loads are applied as point loads at the centroid of each rigid shoe and as uniformly distributed modal loads on flexible shoes in the rigid-flexible virtual prototype model.

Rigid-flexible multi-body model of crawler shoes

Figure 2 shows that the front crawler track is subjected to maximum pressure load in comparison with rear crawler track. The stress distribution in the crawler shoes due to these maximum pressure loads on the shovel front is captured using rigid-flexible multibody dynamics theory as in Figure 4. Two crawler shoes (shoes 8 and 13) or Parts 9 and 14 in the front in Figure 2 are made flexible by importing meshed crawler shoes using modal neutral file (MNF).[13–18] The completed 3-D virtual prototype model for simulating the rigid-flexible crawler-terrain interaction is shown in Figure 5. The virtual prototype model is simulated using MSC.ADAMS/FLEX/DURABILITY to capture crawler-terrain interaction and dynamic stresses induced in the crawler shoes. More details on developing rigid-flexible multibody dynamic model, MNF file generation, mode shapes, stress shapes, modal loads, modal damping, the differential algebraic equations (DAE) governing the rigid-flexible crawler-terrain interaction and modal superposition equations governing nodal stress recovery on flexible crawler shoes can be found in Frimpong et al.[7] The GSTIFF solver with SI2 formulation in MSC Adams is used to integrate DAE's over time with integration error tolerance value E=0.001m.

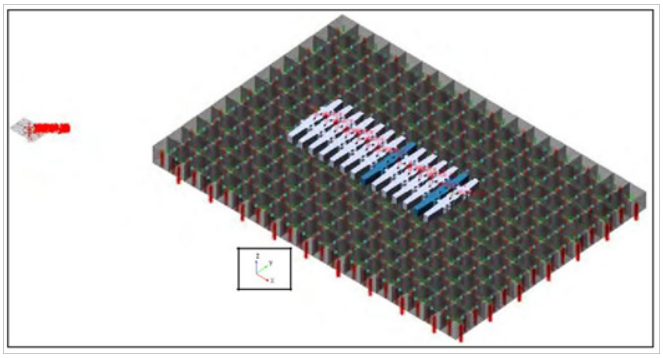

Figure 4 3D virtual rigid-flexible track-terrain interaction prototype.

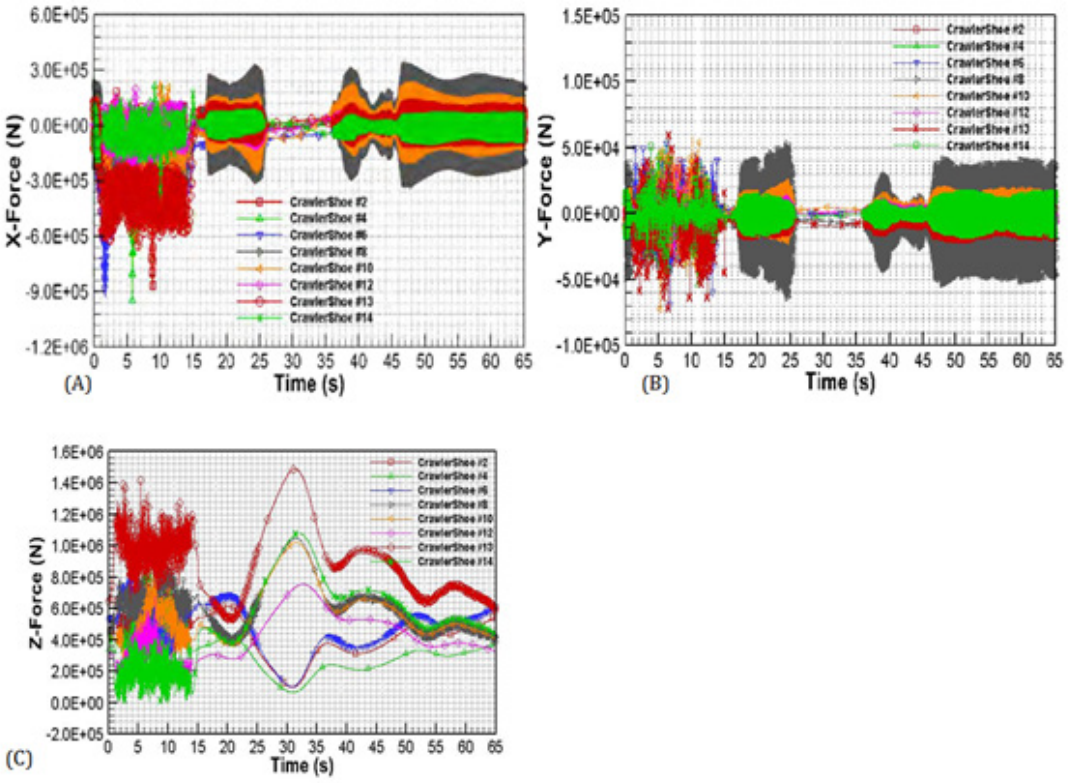

Figure 5 Total contact forces acting on front and rear crawler shoes in the x, y and z-directions.

Citation: Frimpong S, Thiruvengadam M, Gbadam E. Computation and field dynamic stress simulation of shovel crawler shoes. *Material Sci & Eng.* 2018;2(6):241–250. DOI: 10.15406/mseij.2018.02.00065

Table 4 Co-efficients in Equations (4) and (5)

Front crawler shoes		Rear crawler shoes	
a_{0F}	298.7	a_{0R}	157.3
a_{1F}	23.77	a_{1R}	-32.15
b_{1F}	-102.2	b_{1R}	57.06
a_{2F}	-44.05	a_{2R}	33.7
b_{2F}	30.38	b_{2R}	-2.507
a_{3F}	50.28	a_{3R}	-26.95
b_{3F}	14.84	b_{3R}	-24.55
a_{4F}	5.702	a_{4R}	-8.241
b_{4F}	-5.768	b_{4R}	2.2
a_{5F}	-1.506	a_{5R}	-0.6793
b_{5F}	-5.003	b_{5R}	2.534
a_{6F}	-9.745	a_{6R}	2.99
b_{6F}	-0.2056	b_{6R}	6.593
a_{7F}	1.681	a_{7R}	1.233
b_{7F}	1.246	b_{7R}	-2.434
a_{8F}	-0.3779	a_{8R}	-0.3651
b_{8F}	0.262	b_{8R}	-0.6219
w_F	5.422	w_R	5.318

Results and discussions

The total contact forces in the x, y and z directions on different front crawler shoes (8-14) and on the rear (1-7) are shown in (Figure 5). These contact forces are reaction forces due to

i. loading applied on the crawler shoes and

ii. Deformation of the oil sand terrain.

During propel (0<t<15s), large fluctuations in contact forces occur along x, y and z-directions as in Figure 5. The x-contact forces fluctuate between $2.5x10^5$ and $-9.5x10^5$N (Figure 5A). Similarly, y and z-contact forces fluctuate between $6x10^4$ and $-7.2x10^4$ and between $1.4x10^6$ and $1.1x10^3$, respectively as in Figures 5B-5C. During loading, the x-contact force fluctuates between $3.2x10^5$ and $-3.2x10^5$N and y-contact force between $5.2x10^4$ and $-6.3x10^4$N (Figures 5A), (Figure 5B). Due to the semi-static nature of shovel loading (Figure 3), the fluctuations in z-force are negligible in comparison withxand y forces and vary between $1.5x10^6$ and $6.7x10^4$N as in Figure 5C. These contact forces produce the stress loading of the flexible crawler shoes in the front shoes.

Comparison of computed ground force with the field results

The comparison of ground bearing pressure force (N) between field values and computational results for shovel front and rear tracks is shown in Figure 6A. The computational values are obtained by summing the z-contact forces on the respective crawler shoes in the front (8-14) and in the rear (1-7) shown in Figure 6C. It can be seen that the computational results are similar to the field results with a percentage error of 3.5-13% Figure 6B between field and computational values for the front shoes and 6.5-80% for rear shoes. The mean error and the associated standard deviation for the front and rear shoes are 7.7% and 2.0% and 11.8% and 7.7%, respectively. Figure 6B shows a large localized error of 80% on the rear shoes during digging. Simultaneously on the front shoes, the minimum error is 3.5%.

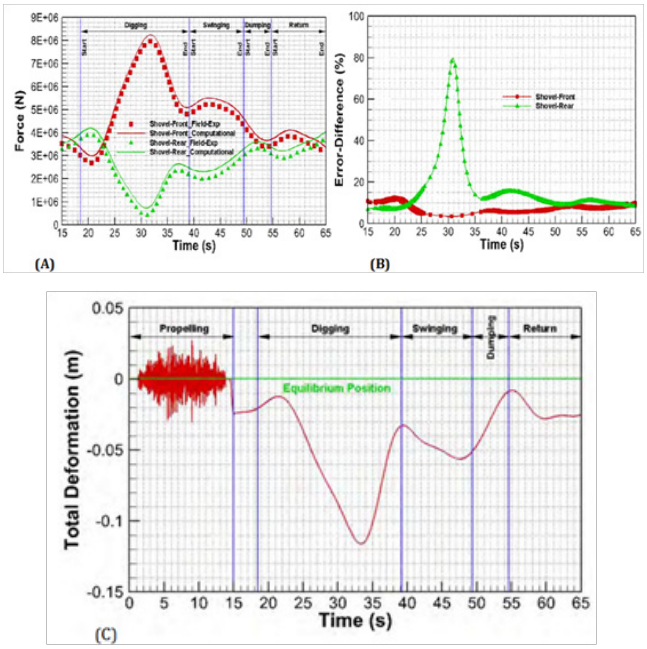

Figure 6 Comparison of ground bearing pressure between field measurements and MSC Adams.

This difference in error between the front and rear shoes is due to the magnitude of ground pressure on the shovel front being 20X larger than the minimum value on the rear shoes during digging. This causes large percentage error for the rear regions as in Figure 6B. The large error discrepancy could also be due to the fact that the rear crawler shoes in are assumed rigid while two front crawler shoes are made flexible (Figure 4). Since the maximum error is within 13% with mean error of 7.7% on the front track with flexible crawler shoes, the resulting stress loading on the shoes should be accurate within 13%. In addition, the computational estimation of ground z-reaction force is consistently larger than the field values, which should over predict the stresses on the flexible shoes and hence can be considered as an accurate estimation for further shoe fatigue study.

Ground deformation

The resulting ground deformation due to shovel propel and loading is shown in Figure 7. During propel, large fluctuations occur with total deformation varying between -2.98 and 2.7cm from equilibrium (t=0) as in Figure 7. Due to the semi-static nature of the applied pressure loads (Figure 3), the total deformation during loading varies smoothly with time as in Figure 7. During loading, the total deformation varies between -11.6 and -0.8 cm. (Figure 7) shows that during loading, the oil sands terrain deforms to a maximum in the digging phase and to a minimum at the end of the dumping phase. The stress distribution in the flexible crawler shoes is obtained by combining modal coordinates or scale factors with stress shapes available in the modal neutral file (MNF) using modal superposition method.[13,14] The time variation of

modal coordinates for mode shapes with frequency (f) in the range of 0 to 1200Hz during propel and loading for flexible crawler shoes 8 and 13 is plotted in Figure 8. The scale factors for mode shapes with frequencies greater than 1200 Hz are negligible. The scale factors show large fluctuations and vary between 0.071 and -0.162 for shoe 8 (Figure 8A) and 0.136 and -0.059 for shoe 13 Figure 8B during both propelling and loading cycle. The results show that mode shape 7 dominates for both flexible shoes with maximum magnitudes of 0.16 and 0.14, respectively.

Dynamic stress contours in the flexible crawler shoes

The von Mises stress distributions of the flexible front crawler shoes 8 and 13 during different stages of propel and loading are shown in Figures 9, Figure 10. The load on the crawler shoes follows the load distribution in Figure 3. The red arrows in Figure 9 indicate contact forces due to interaction between crawler track and oil sands terrain and color contours indicate the von Mises stress in N/m^2 or Pa.

Propelling motion: The von Mises stress distribution during propel is shown in Figure 9. Figure 9A shows that at equilibrium (t=0), the crawler shoe 8 is subjected to large stresses compared to crawler shoe 13. At the beginning of propel, the stresses in the flexible shoes 8 and 13 increase steadily in the acceleration (0<t <5 s) and constant velocity regions (5<t <10 s) and decrease again towards the end of the deceleration phase Figures 9A-9D. The results show that the maximum stress occurs at the joint regions where the shoes are pinned to each other. This is because machine load is uniformly distributed on the shoes and the propel action of the crawler occurs through the joint. The crawler stops at t=15 seconds Figure 9D at which time the loading begins and the track is free to move in all 6-DOF. The stresses in the shoes at the end of propel Figure 9D is dissimilar to that in equilibrium (Figure 9A) even though the crawler is at rest on both occasions. This reveals the dynamic nature of the crawler-oil sands interaction.

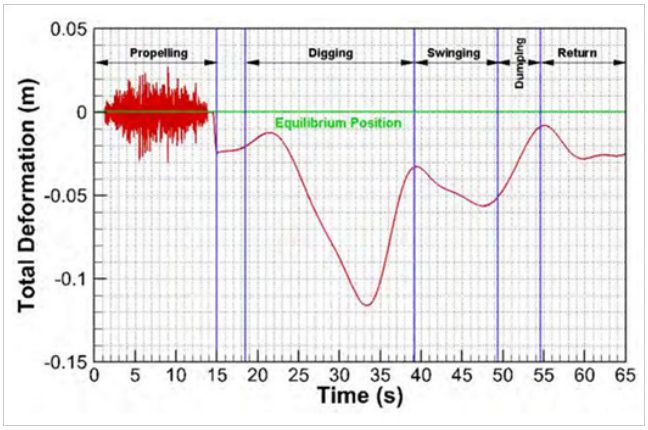

Figure 7 Total deformation of oil sand terrain.

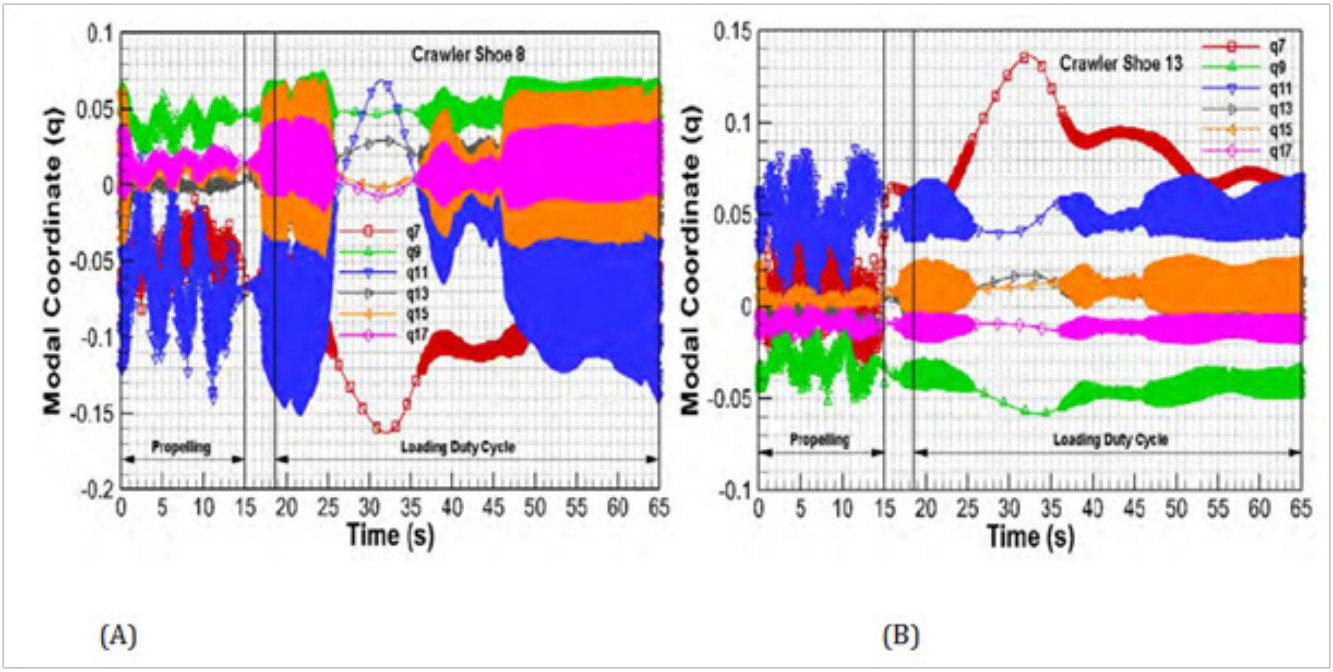

Figure 8 Modal coordinates of flexible crawler shoes 8 and 13.

Loading duty cycle: The von Mises stresses during loading are shown in Figure 10. The von Mises stresses in the crawler shoes during digging (Figures 10A-10C) steadily increase with a maximum occurring at the digging peak at 31.7seconds (Figure 10B). The figure shows that the stress loading in the crawler shoes during swinging, dumping and return (Figures 10D-10F) are small in compared to that during digging. This is due to the relatively large contact or reaction forces (red arrows) at the interface between the shoes and oil sands during digging compared to other loading cycles. The results also show that the maximum stress does not occur in the leading flexible shoe 13 as expected but in the last flexible front shoe 8. This may be due to identical loading of shoes 8-14 (Figure 3) and hence maximum stress loading on crawler shoes depends only on the reaction forces (Figure 5) between oil sand and crawler shoes.

Hot Spots in the flexible crawler shoes

The location of the top 5 hotspots or highest nodal stresses in flexible crawler shoes 8 and 13 during propel and loading is shown

in Figure 11A-11D. The corresponding stresses at these locations, the node numbers and the time at which these hot spots occur are shown in Tables 5, Table 6. From (Table 6), the largest nodal stress of 79MPa occurs during propel in the leading crawler shoe 13. On crawler shoe 8, the largest stress value of 78.5MPa occurs during loading (Table 5). Tables 5, Table 6 also show that the peak stress on shoe 13 during loading is 50% smaller than that on shoe 8. This could be due to the nature of loading. (Figure 11) also shows that crawler shoe hot spots are mostly located around the link pin region and not on the main crawler shoe body. (Figure 12) shows the dynamic variation of the von Mises stresses for the hot spots 1-5 in Tables 5 and 6 for shoes 8 and 13 during propel and loading. The figure shows that during propel, the von Mises stresses for shoe 8 fluctuate between 2.8 and 61.17MPa with an average ranging between 30.3 and 40.7MPa (Figure 12A). The von Misses stresses on shoe 13 also fluctuate between 3.25 and 78.97MPa with an average ranging between 46.1 and 48.0MPa (Figure 12C). During loading, however, the values for shoe 8 vary between 0.32 and 78.5MPa with averages between 15 and 33.2MP (Figure 12B) and, for shoe 13, they vary between 1.67 and 36.7MPa with averages between 13.4 and 28.7MPa (Figure 12D). The maximum von Mises stress induced in the crawler shoes during loading and propel is 79MPa, which is 3X smaller than the yield strength of 250MPa for A36 steel.[19] This dynamic stress (Figure 12) may cause crawler shoe failure at the link-pin joint regions in Figure 11. However, from the field experience, the crawler shoe failure mainly occurred in the roller path area and not around the joint regions. Further investigations must be carried out to determine proper loading on the crawler shoes that can cause hotspot to develop in the roller path area. The crawler shoe loads, from field studies, used in the simulation must be modified to develop hot spots in the roller path area that can be used in the subsequent fatigue study to determine appropriate failure life of crawler shoes.

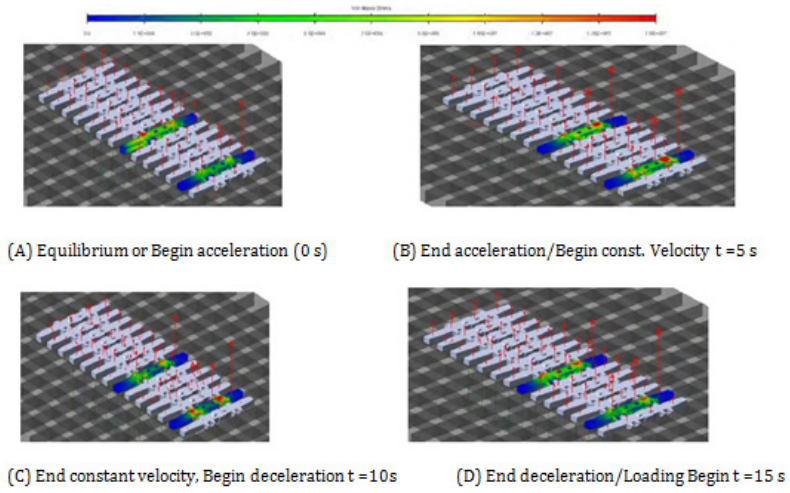

Figure 9 Von-Mises stress contours during propel motion.

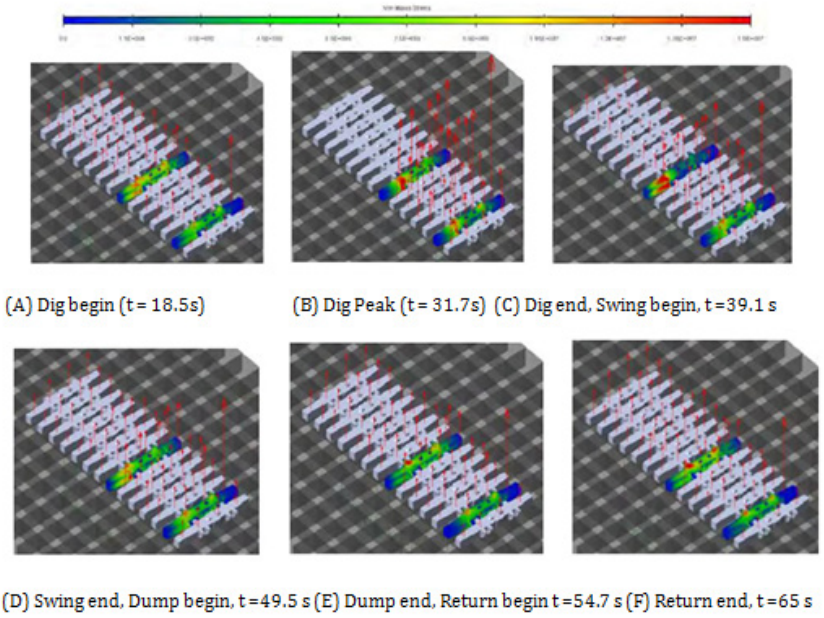

Figure 10 Von Mises stress contours during loading operation.

Citation: Frimpong S, Thiruvengadam M, Gbadam E. Computation and field dynamic stress simulation of shovel crawler shoes. *Material Sci & Eng.* 2018;2(6):241–250. DOI: 10.15406/mseij.2018.02.00065

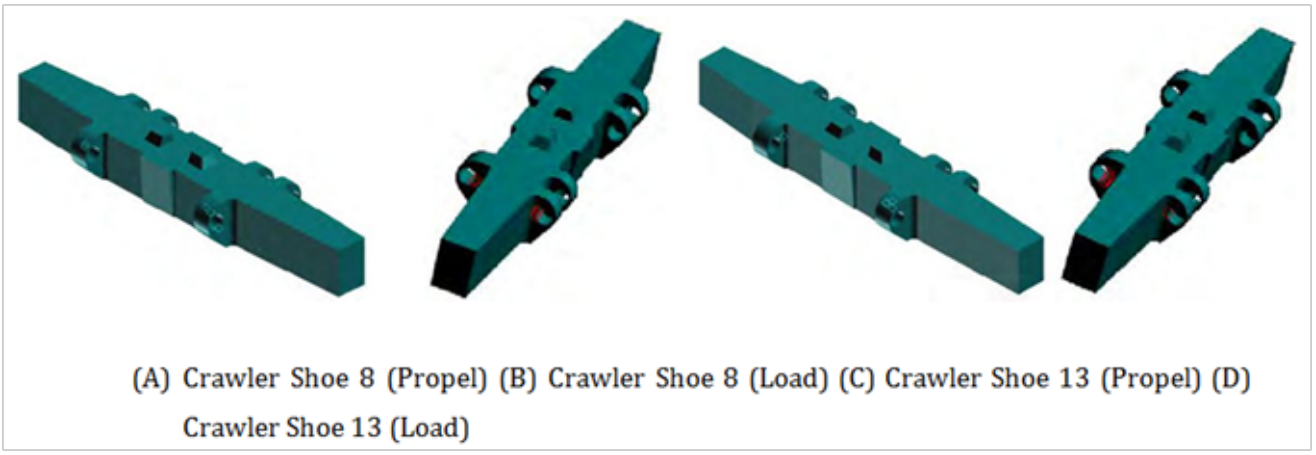

Figure 11 Hot spots location on flexible crawler shoes.

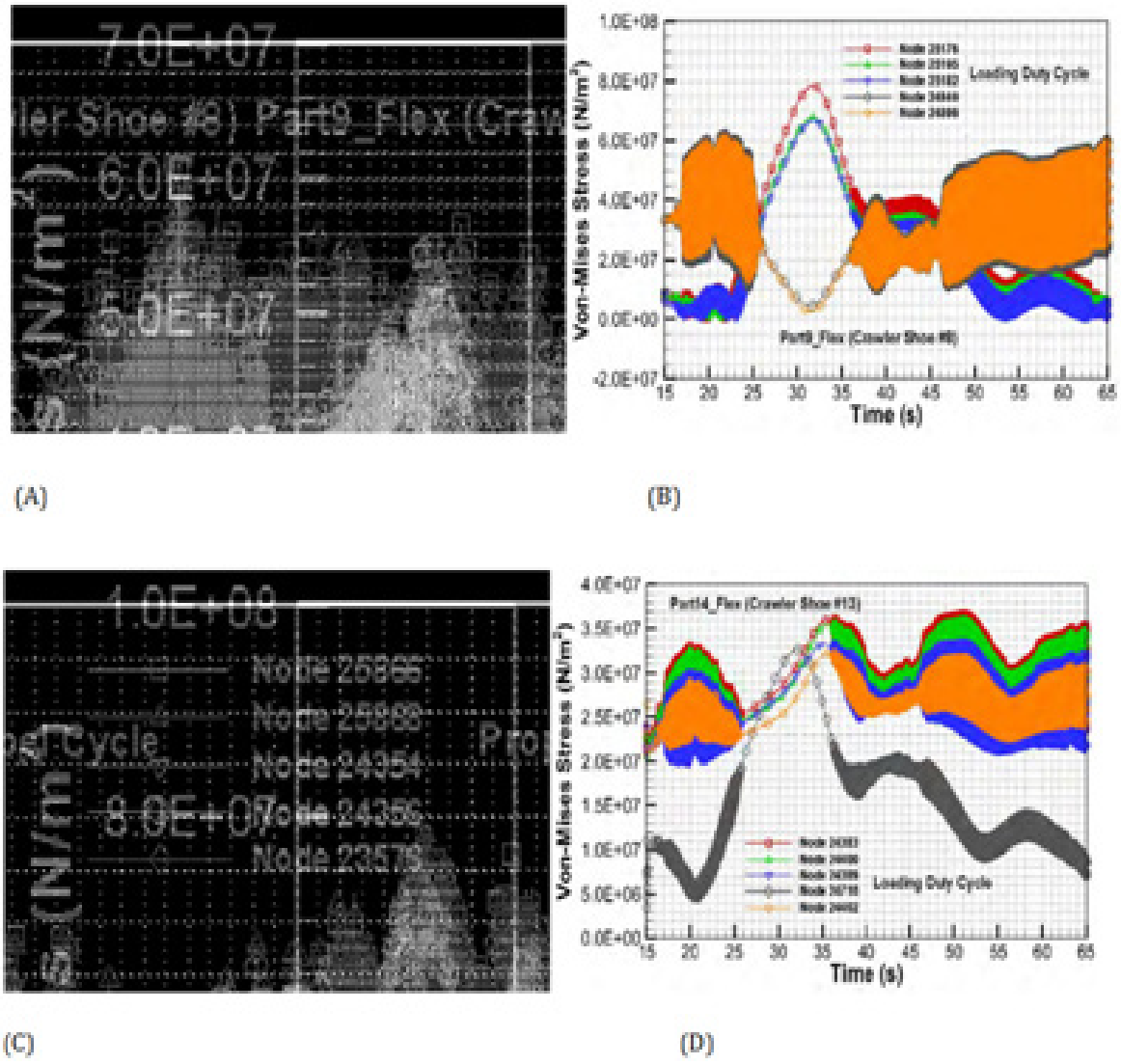

Figure 12 Distribution of hot spot nodes on flexible crawler shoes.

Citation: Frimpong S, Thiruvengadam M, Gbadam E. Computation and field dynamic stress simulation of shovel crawler shoes. *Material Sci & Eng.* 2018;2(6):241–250. DOI: 10.15406/mseij.2018.02.00065

Table 5 Hot spots on Crawler shoe 8

Hot Spot Rank #	Stress (MPa)		Node Id		Time (s)	
	Propel	Loading	Propel	Loading	Propel	Loading
1	61.166	78.454	24438	25176	11.0818	31.76
2	60.805	67.673	24870	25195	11.0818	31.72
3	58.341	66.747	24424	25182	11.0818	31.75
4	54.928	62.148	26334	24849	1.6	21.66
5	54.371	60.873	24820	24866	1.4327	21.66

Table 6 Hot spots on Crawler shoe 13.

Hot Spots Rank #	Stress (MPa)		Node Id		Time (s)	
	Propel	Loading	Propel	Loading	Propel	Loading
1	78.9656	36.7493	25866	24383	1.4754	50.93
2	78.3638	36.0269	25868	24400	1.4724	50.93
3	74.7094	33.6227	24354	24389	1.4724	50.84
4	73.3711	32.6522	24356	24710	1.4724	32.14
5	72.4225	32.3858	23576	24402	1.4724	36.42

Conclusion

The 3-D rigid-flexible virtual prototype model of open crawler track-oil sands terrain interactions is developed in MSC.ADAMS/FLEX/DURABILITY and MSC.NASTRAN to capture dynamic stresses induced in crawler shoes during propel and loading of the P&H 4100C BOSS electric shovel. The crawler shoe loads during propel and loading operations are based on the field measurement data for P&H 4100C BOSS shovel. The propel duty cycle is simulated for 15seconds and it consists of acceleration, constant velocity and deceleration regions. The loading duty cycle is simulated immediately after propel for a period of 46.5seconds.

The cycle consists of digging, swinging, dumping and return operations. The simulation results show large fluctuating contact forces in the x, y and z directions with maximum magnitudes of $9.5x10^5$, $7.2x10^4$ and $1.4x10^6$N during propel and $3.2x10^5$, $6.3x10^4$ and $1.5x10^6$N during loading, respectively. The comparison of ground bearing pressures between field and computed values show maximum errors of 13% and 80% for the front and rear crawler shoes. The maximum oil sands deformation of 11.6cm occurs during digging. The von Mises stresses show that when shovel is propelling, the maximum stress of 79MPa develops in the front crawler shoe 13 at node 25866 during acceleration phase. During loading, the maximum von Mises stress of 78.5MPa develops in crawler shoe 8 at node 25176 during digging. The maximum von Mises stress on crawler shoe 8 during loading is twice that for crawler shoe 13.

The maximum stress, 79 MPa, which is 3X smaller than the yield strength of steel material, develops in the link pin joint regions and not in the roller path area. The ground pressure loads used in this study are from the literature. For a more accurate and realistic study, pressure mats with load cells must be buried under the tracks to record the actual pressures from the shovel tracks in real time. This will cost additional research funds but will yield appropriate results for better characterization. In addition, this study was carried out within oil sands environments, and thus, may not be wholly applicable to other environments. It is therefore recommended that this work be replicated in other harsh environments, such as the iron range formations.

Acknowledgements

None.

Conflict of interest

The author declares no conflict of interest.

References

1. JGI. *4100C BOSS Electric Mining Shovel–AC Drive Product Overview*. USA: © Joy Global Inc; 2012. p. 1–8.
2. JGI. *Electric Rope Shovels*. USA: © Joy Global Inc; 2015.
3. P&H. *Peak Performance Practices: Lower Works*. USA: © P&H Mine Pro; 2005.
4. Frimpong S, Thiruvengadam M. Rigid multi–body kinematics of shovel crawler–formation interactions. int journal of mining. *Reclamation and Environment*. 2015;30(4): 347–369.
5. Frimpong S, Thiruvengadam M. Multi–Body Dynamic Modeling and Simulation of Crawler–Formation Interactions in Surface Mining Operations. *Global Journal of Research in Engineering (F)*. 2015;15(5):29–49.
6. Frimpong S, Thiruvengadam M. Contact and Joint forces modeling and simulation of crawler–formation interactions. *J Powder Metall Min*. 2015;4(135): 1–14.
7. Frimpong S, Thiruvengadam M. Multibody Dynamic Stress Simulation of Rigid–Flexible Shovel Crawler Shoes. *Minerals*. 2016;6(61):1–11.
8. Joseph TG. OsEIPOil: The oil sand equipment interactions program. *CIM*. 2002;95(1064):58–61.
9. Joseph TG, Hansen G. *Oil sand reaction to cable shovels motion*. 2002;95(1064):62–64.
10. Sharif Abadi AD, Joseph TG. Oil sand deformation under cyclic loading of ultra–class mobile mining equipment. *Journal of Terramechanics*. 2010;47(2):75–85.

11. MSC. MSC ADAMS/View Help Document. © MSC, USA; 2014.
12. MSC. MSC ADAMS/Solver Help Document. © MSC, USA; 2014.
13. MSC. MSC ADAMS/Flex Help Document. © MSC, USA; 2014.
14. MSC. MSC ADAMS/Durability Help Document. © MSC, USA; 2014.
15. MSC. MSC NASTRAN Dynamic Analysis User's Guide. © MSC, USA; 2014.
16. Frimpong S, Li Y. Stress loading of cable shovel boom under in–situ digging conditions. *Engineering Failure Analysis*. 2007; 4(4):702–715.
17. Frimpong S, Li Y, Suglo R. Dynamic Torque and Soil Deformation Mechanics and Simulation of the GAP Machinery. *Journal of Powder Metallurgy and Mining*. 2013;2(1): 1–9.
18. MSC. *MSC Software Learning Center*. USA: © MSC Corp; 2016.
19. Harvey P. Engineering properties of steel. American Society for Metals Materials Park, USA; 1982.

Citation: Frimpong S, Thiruvengadam M, Gbadam E. Computation and field dynamic stress simulation of shovel crawler shoes. *Material Sci & Eng.* 2018;2(6):241–250. DOI: 10.15406/mseij.2018.02.00065